Preparation and Properties of Self-Cross-Linking Hydrogels Based on Chitosan Derivatives and Oxidized Sodium Alginate

Guiting Yu, Chunqing Niu, Jiali Liu, Jue Wu, Zheng Jin,* Yiyu Wang,* and Kai Zhao*

Read Online

ACCESS | Metrics & More | Article Recommendations | SI Supporting Information

ABSTRACT: A self-cross-linking and biocompatible hydrogel has wide application potential in the field of tissue engineering. In this work, an easily available, biodegradable, and resilient hydrogel was prepared using a self-cross-linking method. This hydrogel was composed of N-2-hydroxypropyl trimethyl ammonium chloride chitosan (HACC) and oxidized sodium alginate (OSA). A stable and reversible cross-linking network was formed by the Schiff base self-cross-linked and hydrogen bonding. The addition of a shielding agent (NaCl) may weaken the intense electrostatic effect between HACC and OSA and solve the problem of flocculation caused by the rapid formation of ionic bonds, which provided an extended time for the Schiff base self-cross-linked reaction for forming a homogeneous hydrogel. Interestingly, the shortest time for the formation of the HACC/OSA hydrogel was within 74 s and the hydrogel had a uniform porous structure and enhanced mechanical properties. The HACC/OSA hydrogel withstood large compression deformation due to improved elasticity. What's more, this hydrogel possessed favorable swelling property, biodegradation, and water retention. The HACC/OSA hydrogels have great antibacterial properties against *Staphylococcus aureus* and *Escherichia coli* and demonstrated good cytocompatibility as well. The HACC/OSA hydrogels have a good sustained release effect on rhodamine (model drug). Thus, the obtained self-cross-linked HACC/OSA hydrogels in this study have potential applications in the field of biomedical carriers.

Strain-strain curve of ten successive loading-unloading cycles of hydrogel
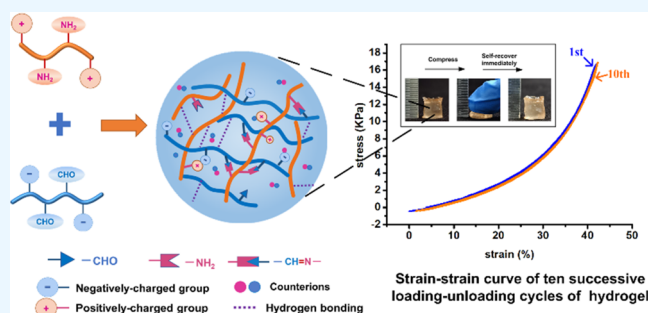
1. INTRODUCTION

Hydrogel is a kind of functional polymer material with special adsorption ability to water. Its three-dimensional (3D) polymer network is similar to the natural extracellular matrix (ECM) structure and has good biocompatibility.[1] It is widely used in tissue repair, biomedicine, and drug-controlled release fields.[2] In particular, hydrogels prepared from natural polysaccharides have greater development potential because of their excellent biocompatibility and degradability. Various polysaccharide polymers, such as chitosan (CS), sodium alginate (SA), hyaluronic acid, cellulose, etc.,[3−5] can form hydrogels through physical or chemical cross-linking methods.[6−10] Due to its excellent biocompatibility, biodegradability, and wide range of sources, it has attracted the attention of researchers and is widely used in the preparation of functional hydrogels.[11,12] However, for biomedical materials, the cross-linked networks produced by general chemical cross-linking inevitably introduce toxic chemical reagents or undergo complex preparation processes.[13,14] Physical cross-linked hydrogels also exhibited other deficiencies due to the weak cross-linking network, uneven distribution of polymer cross-linking, and difficulty in controlling the degree of cross-linking, which can limit the application of such traditional hydrogels in biomedical fields. Therefore, developing a method to produce self-cross-linked hydrogels with injectability in situ, a stable

cross-linking network, and desirable resilience self-healing is crucial for effective biomaterial applications.

SA is a natural biocompatible polysaccharide polymer; parts of its constitutional units can be oxidized to aldehyde groups through ring opening reactions to become oxidized sodium alginate (OSA) under an oxidizing environment.[15] The OSA with a large number of hemiacetal groups can react with many groups, such as amines, and some dynamic covalent bonds are formed. For example, Wang et al. constructed an injectable, bioresponsive, and self-healing hydrogel based on OSA and hydrazide-modified poly(ethylene glycol) (PEG), formed by Schiff base reaction with good injectability.[16] What's more, previous studies on OSA-based composite hydrogels have shown that combining OSA with other polymers can provide superior performance, including excellent biocompatibility, controlled biodegradability, and better reactivity, and can be quality-metabolized.[17−20] However, the current series of
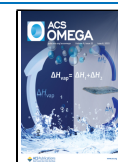
hydrogels prepared based on OSA still have certain defects, such as significantly weaker cross-linking of divalent ions, uncontrollable cross-linking reactions, and very weak mechanical strength.[21] OSA as an anionic polymer, the molecular chain not only includes residues of carboxyl and hydroxyl groups that can form polyelectrolyte complexes with polycations (such as poly-L-lysine, CS)[22] but also contains oxidized aldehyde groups that can cross-link with polymers with amino groups by Schiff base self-cross-linking, thus improving the cross-linked reaction to improve the mechanical strength.

Due to their straightforward procedure and capacity to produce reversible chemical bonds, Schiff base self-cross-linked reaction hydrogels have also received a lot of attention recently. For example, Zhou et al. designed an injectable hydrogel based on aldehyde-functionalized chondroitin sulfate mixed with gelatin in the presence of borax to form dynamic Schiff base bonds.[23] A novel hydrogel is prepared using multialdehyde guar gum (MAGG) and N,O-carboxymethyl chitosan (CMCS) for the sustained delivery of anticancer drugs through dynamic Schiff base bonds.[24] A hybrid hydrogel composed of aminated collagen (AC), OSA, and antimicrobial peptides (polymyxin B sulfate and bacitracin) is developed to promote full-thickness wound healing.[17] In addition, some hydrogels are formed by dynamic interactions between groups with opposite charges and can exhibit excellent mechanical properties under the partial shielding effect of certain salt ions. For instance, Yuan's team used negatively charged monomeric acrylic acid in a positively charged polysaccharide 2-hydroxypropyl trimethyl ammonium chloride chitosan solution, partially shielded by sodium chloride salt ions, to synthesize a physical hydrogel with a high-density dynamic ion-bonded compact structure, exhibiting good mechanical and electrical conductivities.[25] By using hydrogen-bonding and electrostatic interactions between polyanions and polycations, Geng's research group created hydrogels with a homogeneous structure in order to equalize the charge and create uniform and clear hydrogels; sodium chloride was added to the gel system.[21] Therefore, the hydrogels formed by Schiff bases of self-cross-linked reaction between cation and anionic polymers can be achieved by shielding partial effects of certain salt ions.

N-2-Hydroxypropyl trimethyl ammonium chloride chitosan (HACC) is a product obtained by reacting 2,3-epoxypropyl-trimethylammonium chloride (EPTAC) with chitosan. HACC has a higher positive charge density, a large number of amino groups,[26] good water solubility,[27] antibacterial properties,[28,29] and biocompatibility. Gan et al. developed a poly(vinyl alcohol)-(2-hydroxypropyl trimethyl ammonium chloride chitosan) (PVA-HACC) DN hydrogels without organic solvents or toxic to excellent mechanical properties.[4] For the sequential treatment of diabetic wounds, Qi et al. developed an "all-in-one" in situ-injectable hydrogel using quaternized chitosan and oxidized β-glucan in a Schiff base reaction with polydopamine nanoparticles.[26] As a result, we believe that HACC can provide sufficient amino groups for the Schiff base reaction with OSA, making the preparation of a novel polysaccharide hydrogel possible.

As far as we know, HACC/OSA-based hydrogels have not been reported yet. Based on the above considerations, we hypothesize that after the shielding part of the charge, the flocculation problem caused by the strong electrostatic interaction between cationic and anionic polymers can be avoided, and the homogeneous hydrogel can be obtained by

the Schiff base reaction. In this study, a self-healing was established based on HACC and OSA by combining Schiff base self-cross-linked with hydrogen bonding under the partial shielding effect of counterions from NaCl. By analyzing the hydrogel time, mechanical characteristics, swelling dynamics, degradability, drug sustained release, and antibacterial ability, we can affirm that a new approach for the creation of self-cross-linked hydrogel based on natural polysaccharide derivatives has been established, which has possible uses as a biomedical carrier or an antibacterial wound dressing.

2. EXPERIMENTAL SECTION

2.1. Materials. Sodium periodate, SA (viscosity = 0.02 (10 g/L 20 °C)/(Pa·s); M_w = ~700 kDa), and glycol were all provided by Sinopharm Chemical Reagent Co., Ltd. (China). Sodium tetraborate was purchased from Lingfeng Chemical Reagent Co., Ltd. (Shanghai, China), chitosan (CS) (M_w = 100 kDa) was purchased from Shanghai Macklin Biochemical Co., Ltd., and 2,3-epoxypropyl trimethyl ammonium chloride was supplied from Rhawn reagent Co., Ltd. (Shanghai, China).

2.2. Preparation of the HACC. 60% of D.S. HACC is synthesized. To put it simply, 6 g of CS was dissolved in a certain amount of acetic acid solution, stirred evenly for 1 h, and then 15 mol/L of NaOH solution was added drop by drop, adjusted to pH = 9, soaked for 0.5 h, filtrated, precipitated, washed to neutral, and vacuum freeze-dried to obtain the pretreated CS. The pretreated CS was dispersed in 50 mL of isopropyl alcohol solution, and epoxypropyl trimethyl ammonium chloride isopropyl alcohol solution (8 g/50 mL) was gradually added under the condition of an 80 °C water bath. After 9 h of reaction, the CS was repeatedly washed with anhydrous ethanol, filtered, and freeze-dried to constant weight, and then HACC was obtained. The product was characterized by ^1H NMR and Fourier transform infrared spectroscopy (FTIR). The measurement of degrees of substitution can be seen in the Supporting Information (SI).

2.3. Synthesis of the OSA. The oxidation of SA was carried out in aqueous solution using $NaIO_4$ as the oxidant to prepare the OSA with various theoretical oxidation degrees (ODs) based on the reported methods.[15] In a beaker, briefly, 8 g of the SA was completely dissolved in 400 mL of pure water and then under vigorous stirring to obtain 2.0% (w/v) of SA solution. Afterward, a certain amount of $NaIO_4$ was added to initiate the oxidation reaction at 25 °C to obtain OSA. The reaction was performed for a period of 24 h, and these reactions were stopped by the addition of equimolar ethylene glycol under stirring for 0.5 h to reduce the excess periodate. Then, they were placed in the dialysis bag with a molecular weight cutoff of 3500 to dialyze against deionized water for 3 days. Finally, the dried OSA was obtained by freeze-drying. Determination of the oxidation degree (OD) of OSA is seen in the SI. In this paper, OSAs with a theoretical OD of 0.4 and 1 were prepared and named OSA-0.4 and OSA-1, respectively, according to the molar ratio of $NaIO_4$ to SA.

2.4. Synthesis of the HACC/OSA Hydrogels. HACC was added to distilled water at a concentration of 5 wt %. OSA was dissolved in a 0.2 mol/L borax solution at a final concentration of 5, 10, 15, and 20 wt %; then, some NaCl were added to the HACC solution at a final concentration of 3 wt %; the HACC solution after partial charge shielding was obtained by completely stirring.[25] A series of OSA with different ODs and concentrations were quickly added to the HACC solution, and then the stirred well mixture was placed

at 37 °C for a period of time before forming hydrogels. The HACC and OSA were mixed in a volume ratio of (2−5):1; the ultimate hydrogel obtained was named HACC/OSA-*m*-*n* (*m* is the OD of OSA and *n* is the different concentrations of OSA, which are 5, 10, 15, and 20%). A series of HACC/OSA hydrogels were prepared in this study, and the gelation time was determined by an inverted tube test at 37 °C.[30]

2.5. FTIR and ¹H NMR Spectroscopy Analysis and Rheological Behavior. To verify the synthesis of HACC, OSA, and HACC/OSA hydrogels, various raw ingredients and produced hydrogels were measured using Fourier transform infrared spectroscopy (FTIR). An FTIR spectrometer (Nicolet 5700, Thermo Fisher Electron Corporation) was used to record data on a variety of substances, with 32 cumulative scans collected in the range of 500−4000 cm⁻¹ against the background of blank KBr particles. The spectral resolution of the infrared spectrometer is better than 0.4 cm⁻¹.

Proton-nuclear magnetic resonance (¹H NMR) spectra of samples were recorded in a deuterium oxide solution on a Bruker, AVANCE III HD 400, (Germany) at 400 MHz to record changes in functional groups before and after modification of polysaccharides.[26]

A modular compact rheometer MCR 102 (Anton Paar) was used for the rheological test of HACC/OSA-1 (10, 15, and 20%). Briefly, to establish the limit of the linear viscoelastic area, hydrogels were exposed to dynamic amplitude strain scans at a fixed constant angular frequency of 6.28 rad/s (1 Hz) at a temperature of 25 °C. With a frequency sweep range of 0.6−56 rad/s, dynamic oscillatory frequency scans were carried out under continuous strain. The hydrogel's viscosity was evaluated at shear rates ranging from 0.15 to 100 s⁻¹ and angular frequencies of 6.28 rad/s.

2.6. Morphological Characterization. The morphology of the hydrogels was characterized by freeze-drying the hydrogels at −80 °C and gold-plated for about 90 s using an SBC-12 mini-ion sputterer (Cressington KYKY Technology. Beijing, China). The morphology under an accelerating voltage of 3.5 kV was observed using a scanning electron microscope (SEM) (Pro-SE, Phenom).

2.7. Macroscopic Self-Healing Experiments. In order to verify the macroscopic self-healing ability of HACC/OSA hydrogels, we carried out the method by placing two pieces of hydrogels on top of each other. Briefly, HACC/OSA hydrogels were prepared in molds and one piece was stained with rhodamine B (RB). Two pieces of hydrogels were placed on top of each other and exposed to air at room temperature. The pieces were brought into physical contact with each other without applying pressure, and the self-healing effect of the hydrogels was observed after a period of time.

2.8. Compressive Properties. HACC/OSA was prepared in a fixed mold at 37 °C to obtain a cylindrical hydrogel sample with a diameter of 6 mm and a height of about 7 mm. The compressive modulus of the hydrogel at room temperature was tested using a mechanical testing system and a 50 N load cell. The specimen compresses the hydrogel at a regular deformation charge of 1.0 mm/min until the stress reaches the yield point. From the initial dimensions of the specimen, the load and displacement data were converted to stress−strain values, and the compressive modulus (*E*) was determined using the slope of the initial linear region of the stress−strain curve.

2.9. Swelling Kinetics, Degradation *In Vitro*, and Moisture Content. The swelling kinetics of the hydrogel was

characterized by monitoring the mass change during the culture. The hydrogel was trimmed into a regular shape, and the initial mass of the hydrogel (m_d) was weighed after freeze-drying and soaked in a 0.01 mol/L phosphate-buffered saline (PBS) at 37 °C. The swollen hydrogel was removed at specific checkpoints and weighed (m_t) immediately after absorbing excess liquid on the surface with filter paper. The swelling ratio was calculated

$$\text{swelling ratio} = \frac{m_t - m_d}{m_d}$$

The degradation behavior of hydrogel dressings was characterized by monitoring mass loss. The initial hydrogel weighed (w_0) was immersed in PBS containing 0.01 mol/L of lysozyme and placed in a constant temperature shaking table (37 °C, 100 rpm). At the measurement time point, after washing away the residual PBS, the hydrogel was removed and lyophilized and weighed (w_t), and its *in vitro* degradation weight retention ratio was calculated

$$\text{weight retention ratio} = \frac{w_t}{w_0} \times 100\%$$

The water content of the hydrogels was determined by freeze-drying. A cylindrical hydrogel sample was prepared in a fixed mold, the surface water was absorbed with a filter paper, its wet weight (w_0) was accurately weighed, and it was put in a freeze-drying box to dry for 24 h, which was dried and equilibrated for 12 h; it was taken out quickly after constant weight. And the dry weight (w_1) was accurately weighed. The moisture content of the hydrogel can be calculated from its wet weight and dry weight

$$\text{moisture content} = \frac{w_0 - w_1}{w_0} \times 100\%$$

2.10. *In Vitro* Drug Release. RB was used as a model drug to assess the *in vitro* release properties of the hydrogels. Different hydrogels were prepared; 200 μg of RB was added to 1 mL of hydrogel system, and 5 mL of PBS (pH = 7.4) was added after the hydrogel was completely solidified, shaken in a shaker at 37 °C, 100 rpm, and 1 mL of release solution was removed at a fixed time point and supplemented with 1 mL of fresh PBS, and the release solution was measured at 554 nm on a Thermo LabSystems Microplate Reader (SpectraMax 190, Molecular Devices) for RB release The concentration of RB was measured at 554 nm on a Microplate Reader, and the cumulative release was calculated.[31]

2.11. Cytotoxicity Test. The cytotoxicity of the hydrogels was assessed by preparing the extracts and using the methods previously reported.[31] Bone marrow mesenchymal stem cells (BMSCs) were extracted from the bone marrow of Sprague-Dawley rats (3−5 weeks old, 90 g) based on previously reported methods.[32,33] All animal experiments were authorized by the Teaching and Research Animal Care and Use Committee of Taizhou University. BMSC cells were cultured in 96-well plates by adding 100 μL of cells at a density of 1 × 10⁴ cell/mL per well. After incubation for 24 h at 37 °C in a 5% CO₂ incubator, the normal medium was replaced with medium extracts of different hydrogel samples. The normal medium was maintained under the same conditions and served as a negative control. First, we used the HACC/OSA-15% hydrogel extract to conduct the cytotoxicity test with CCK-8 (Mlbio, Shanghai, China) method at different concentrations
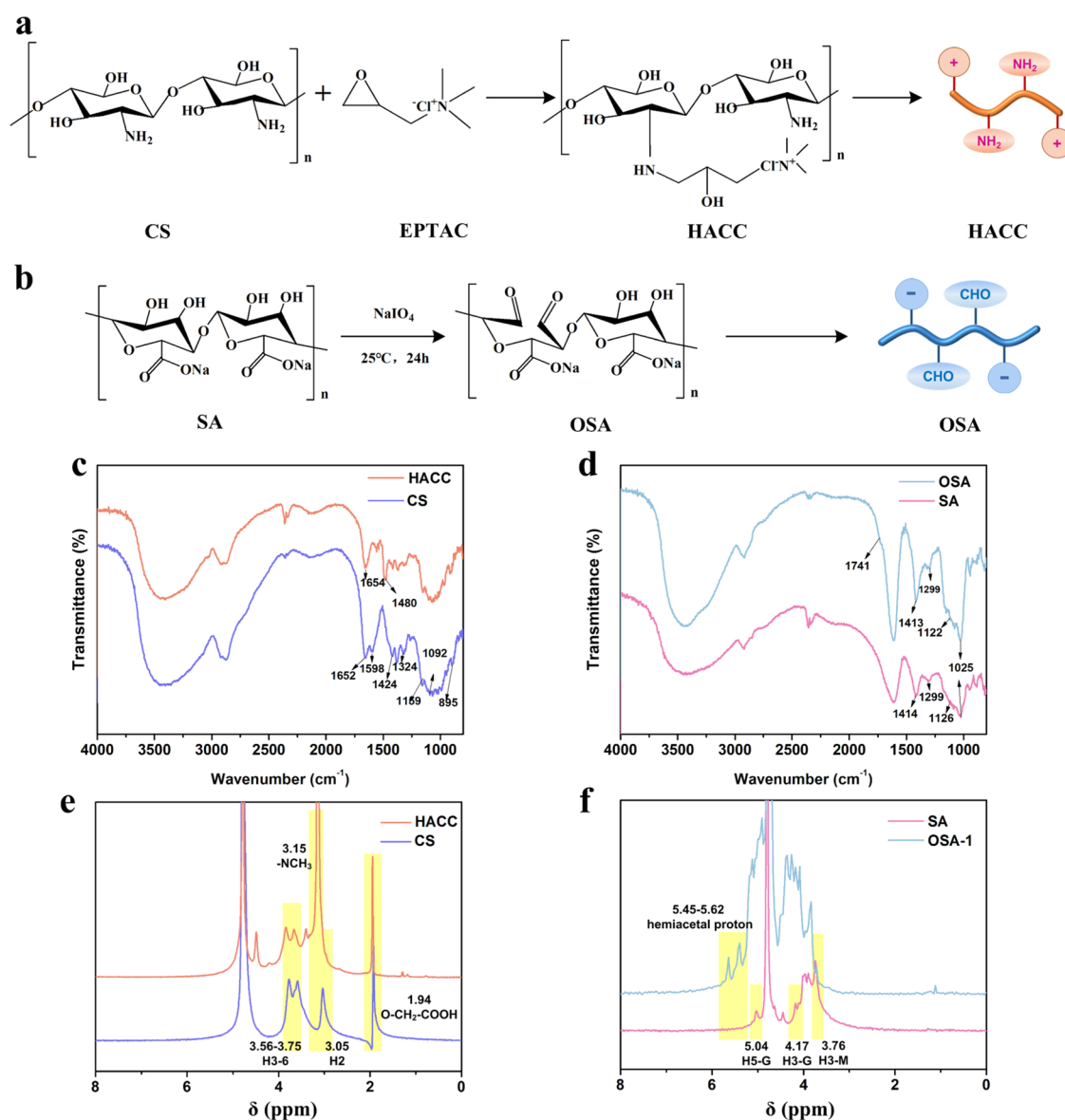
Figure 1. (a) Synthetic route of the HACC and (b) synthetic route of OSA, (c) FTIR spectra of the CS and HACC, (d) FTIR spectra of the SA and OSA-1;, (e) ^{1}H NMR spectra of the CS and HACC, and (f) ^{1}H NMR spectra of the SA and OSA-1.

(0, 20, 40, 60, 80, 100 mg/mL) and other samples were evaluated after determining the extract concentration of cell viability. At the indicated time points (1, 2, and 3 d), cells were assessed for viability using the CCK-8 method and cell viability was calculated by measuring OD values at 450 nm using a Microplate reader. On the third day, the cells were cultured, dyed with a fluorogenic stain (Hoechst 33342/PI, Beyotime), and visualized by fluorescence microscopy.

2.12. Antibacterial Efficiencies of the HACC/OSA Hydrogels. *Escherichia coli* and *Staphylococcus aureus* were used as model bacteria to evaluate the antibacterial properties and bactericidal efficacy of the composite hydrogels by the colony method. Sterile hydrogels were prepared in 48-well plates, 10 μL of bacterial suspension (10^7–10^8 CFU/mL) was added, incubated at 37 °C for 2 h, and then the bacteria were resuspended in 1 mL of physiological saline; 100 μL of bacterial suspension was taken and incubated on LB agar plates for 18 h. Active bacteria are expressed in colony forming units per milliliter (CFU/mL) to calculate the antibacterial rate

$$\text{antibacterial rate (\%)} = \frac{\text{number}_{\text{control}} - \text{number}_{\text{samples}}}{\text{number}_{\text{control}}} \times 100\%$$

SEM images were used to further illustrate the changes in bacterial morphology before and after hydrogel treatment.[34] Briefly, the treated bacterial samples were fixed with 2.5% of glutaraldehyde for 6 h and then dehydrated with different concentrations of ethanol (30, 50, 70, 80, 90, 100%), dropped on silicon wafers, dried, and observed after sputtered gold.

3. RESULTS AND DISCUSSION

3.1. Synthesis and Characterization of the HACC and OSA. The HACC with better water solubility was obtained by the modification reaction between CS and EPTAC (Figure 1a), and the degree of substitution was determined to be about 60%. Two different determinations of the oxidation degree (OD) of OSA (0.4 and 1) were prepared by the reaction of SA with sodium periodate (Figure 1b). The actual OD of OSA
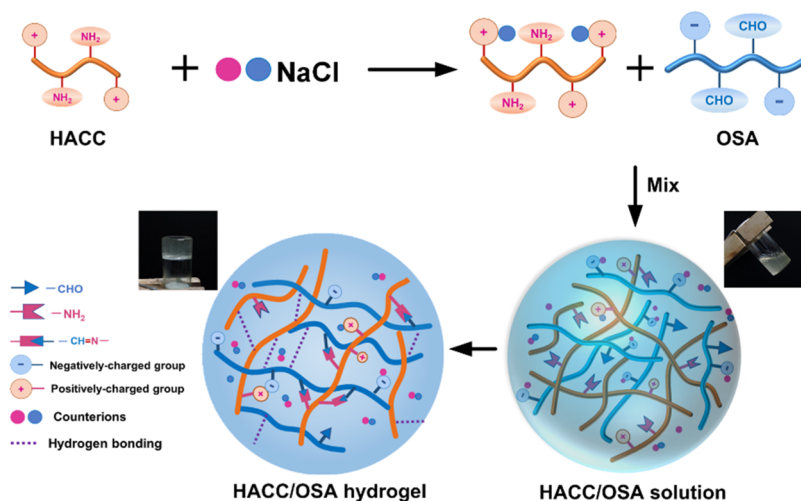
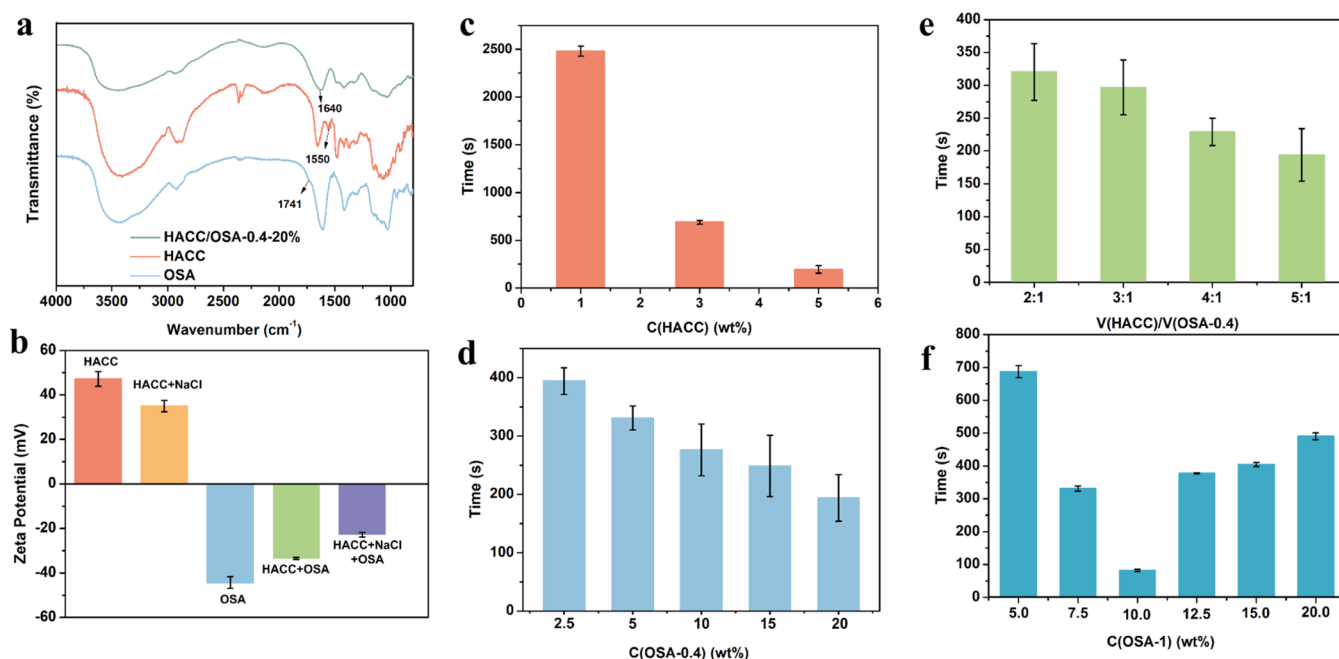**Figure 2.** Process of composite gelation shown schematically.

Figure 3. (a) FTIR spectra of the HACC, OSA, and HACC/OSA-0.4-20% hydrogels; (b) ζ-potential of different component solutions. Effects of different parameters on gelation time; (c) HACC concentration; (d) OSA-0.4 concentration; (e) volume ratio of OSA-0.4 to HACC; and (f) OSA-1 concentration ($n = 3$).

was calculated as 0.38 and 0.80 according to the test method in the SI. The structure of HACC and OSA was confirmed by comparing the FTIR spectra. Compared with the CS, the FTIR spectrum of HACC (Figure 1c) shows a C−H bending vibration absorption peak at 1480 cm^{-1}, while the N−H bending vibration absorption peak at 1598 cm^{-1} disappears, indicating that EPTAC was successfully connected to it. Comparable to SA, a new absorption peak at 1741 cm^{-1} was observed (Figure 1d). This peak was attributed to the C=O stretching vibration of the aldehyde functional group of OSA and also demonstrated that NaIO$_4$ had converted the adjacent hydroxyl groups at the C-2 and C-3 positions on the SA backbone to the aldehyde groups.[15,20] Not only that, we further confirmed the successful preparation of HACC and OSA by ^{1}H NMR spectra, The results of the ^{1}H NMR spectra of CS and HACC are shown in Figure 1e. The strong signal

characteristic peaks at 3.05 and 3.56−3.75 ppm for CS belonged to H-2 and H-3-6 of the glucosamine ring, and the signal characteristic peaks at 1.94 ppm belong to O-CH$_2$-COOH, and for HACC, the ^{1}H NMR spectra, the characteristic peak at 3.15 ppm corresponds to -NCH$_3$, indicating the presence of HACC, indicating that EPTAC was grafted to the chitosan chain.[35] As shown in Figure 1f, the signals observed at 5.04 ppm in the SA sample correspond to the peak of H5-G. The signals observed at 3.76 and 4.17 ppm correspond to H3-M and H3-G, respectively. However, in the spectrum of sample OSA-1, two new signal peaks appear at 5.62 and 5.45 ppm, which would correspond to a hemiacetal proton formed by an aldehyde and a neighboring hydroxyl group, indicating the successful preparation of OSA; this is consistent with literature reports.[3,16]
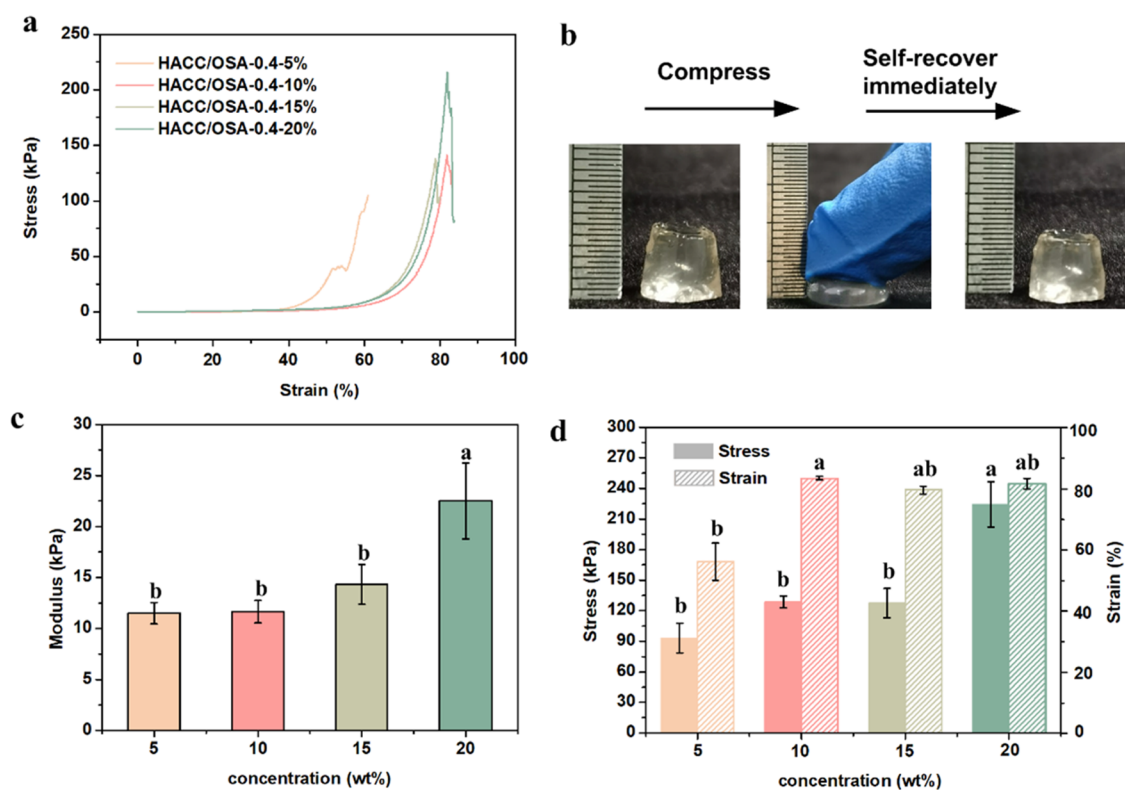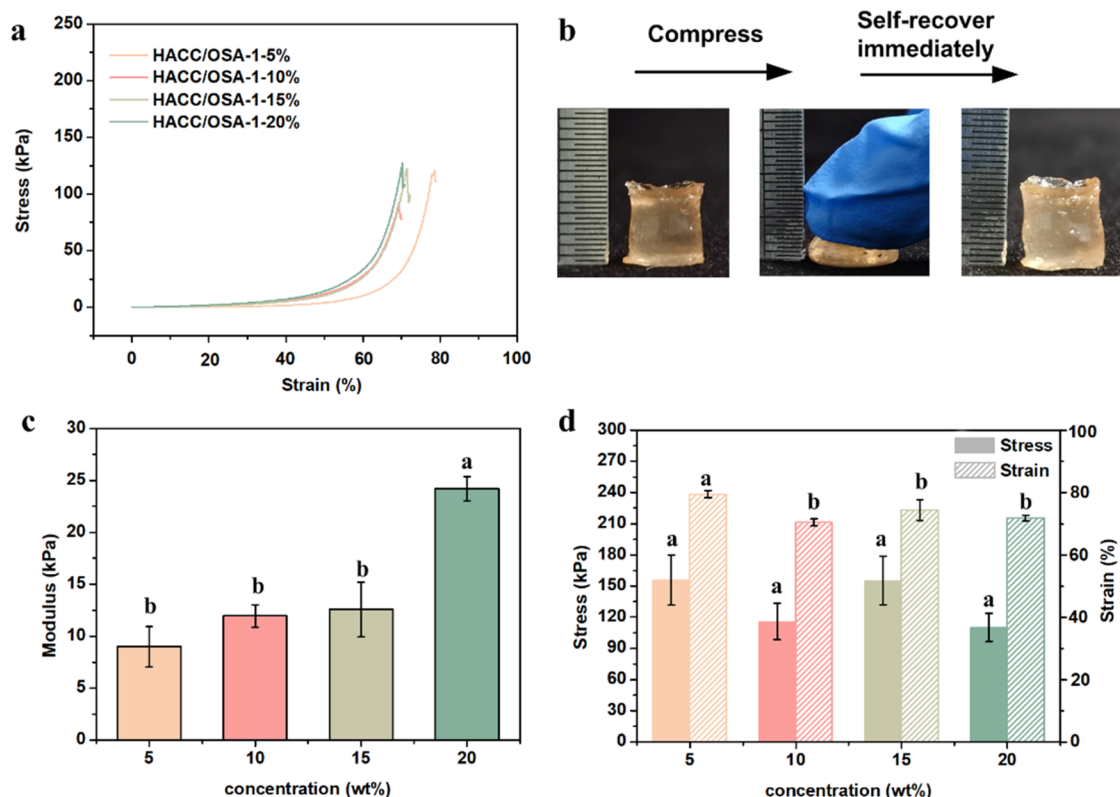
Figure 4. Stress−strain curve and compressive modulus determination of the HACC/OSA-0.4. (a) Stress−strain curves of the HACC/OSA-0.4 hydrogels. (b) Recoverable compression test of the prepared hydrogels. (c) Compressive modulus of HACC/OSA-0.4 hydrogels. (d) Stress−strain of HACC/OSA-0.4 hydrogels with different concentrations. Different alphabets in the figure denote significant variation (n = 3, ± standard deviation, $p < 0.05$).

3.2. Preparation of Hydrogel. Figure 2 describes the synthesis procedure of HACC/OSA hydrogels. First, the cation electronegativity in HACC solution is weakened by the partial shielding effect of counterions from NaCl; OSA was dissolved under the action of 0.2 mol/L borax, the addition of borax to OSA formed a boron−diol complex, resulting in OSA chains that are linked at multiple points and remain soluble, thus accelerating the gelation of the hydrogel.[23] The HACC solution was mixed with different OSA solutions to form a series of hydrogels by the combination of Schiff base cross-linking and hydrogen bonding. In this dynamic cross-linking network, the amino groups of the HACC and the aldehyde groups in OSA are cross-linked by the Schiff base reaction to form dynamic imino bonds. Moreover, the molecular chain of OSA contains many hydroxyl (−OH) and aldehyde (−CHO) groups that can form hydrogen bonds, and the molecular structure of HACC has amino groups that can also form hydrogen bonds. Therefore, due to these chemical properties, hydrogen bonds are formed between HACC and OSA.[36,37] The precursor solution of hydrogel is precipitated due to the strong electrostatic interaction between the positive and negative charges from the two precursors in the absence of counterions from NaCl. Thus, the precipitates of the hydrogel precursor solution resulted in the inability to form a homogeneous hydrogel. After adding NaCl, the precipitation in the precursor solution disappeared (Figure S1). The result may be due to the fact that the polymeric polyelectrolytes in the precursor solutions contain strong positive and negative charges, and when comingled, precipitation rapidly occurs via electrostatic interaction, which can be regulated by adding counterions from NaCl to solve the problem of precipitation.[25]

However, in this system, as hydrogen bonding is relatively weaker than ionic interaction, it might not cause the flocculation problem by mixing the polymers. We further demonstrated the shielding effect of counterions of NaCl by measuring the ζ-potential. Figure 3b shows that the ζ-potential of cationic HACC decreases from 47.2 to 35.0 after adding counterions from NaCl, indicating that the addition of NaCl can shield the charge of the polyelectrolytes in solution. And the anionic polysaccharide, OSA solution exhibited a negative ζ-potential at −44.3, and when HACC$^+$ solution was added to the OSA$^−$ solution, flocculation was immediately observed, and the solution after the removal of precipitation presented a negative ζ-potential at −33.5; after adding NaCl, the ζ-potential of the HACC/OSA solution turned to be −22.8. The results indicate that the electrostatic association between the oppositely charged polymers is very strong, which is consistent with the previous literature.[38] However, with the addition of the counterions, NaCl and Cl$^−$ can competitively bind to HACC$^+$ to form a more stable complex without flocculation and Na$^+$ can also bind to OSA$^−$ offset part of the negative charge, resulting in a less negative ζ-potential in the system. NaCl was added to weaken the strong electrostatic interaction between HACC and OSA, which solved the flocculation problem caused by rapid gel formation. In higher salt concentrations, the ions shielded the charge of polyelectrolytes in solution, disfavoring the electrostatic interactions, and then, the importance of nonelectrostatic forces on complexation increases.[39] In our study, the shielding effect of counterions of NaCl effectively helped the Schiff base reaction to occur.

A series of HACC/OSA hydrogels were obtained by forming a stable and reversible cross-linked network in situ through

Figure 5. Stress−strain curve and compressive modulus determination of the HACC/OSA-1. (a) Stress−strain curves of HACC/OSA-1 hydrogels. (b) Recoverable compression test of the prepared hydrogels. (c) Compressive modulus of HACC/OSA-1 hydrogels. (d) Stress−strain of HACC/OSA-1 hydrogels. Different alphabets in the figure denote significant variation ($n = 3$, $\pm$ standard deviation, $p < 0.05$).

Schiff bases and hydrogen bonding, and the state of the hydrogel before gelation is a solution state, and after gelation, it is inverted and does not flow. To confirm the structure of the hydrogel, the HACC/OSA-0.4-20% hydrogel was characterized by FTIR (Figure 3a). The N−H vibrational peak at 1550 cm^{-1} vanished in HACC, while the characteristic peak of the aldehyde group at 1741 cm^{-1} disappeared in OSA, and the absorption peak at 1640 cm^{-1} broadened, which was attributed to the "N=C" (imino bond) stretching vibrational peak,[40,41] indicating that the hydrogel was successfully cross-linked by the Schiff base reaction between the OSA and HACC.

3.3. Gelation Time Results. The gelation time was examined systematically in this research. For hydrogels with the same ratio and the same concentration of OSA-0.4, the results of the effect of HACC concentration on the gelation time of HACC/OSA hydrogels are shown in Figure 3c. As the concentration of HACC increased, the gelation time of the hydrogel decreased from 2480 ± 53 to 194 ± 40 s. This may be because more amino groups from the HACC can be provided for the Schiff base reaction, leading to a faster cross-linking reaction. Figure 3d illustrates the effect of the variable concentration of OSA-0.4 on the gelation time when the concentration of HACC and other conditions remain unchanged. The gelation time became shorter and shorter with the increase of the OSA-0.4 concentration. When the OSA concentration was 2.5 wt %, its gelation time was 394 ± 23 s, while the gelation time could be shortened to 194 ± 40 s as the concentration of OSA-0.4 reached 20 wt % because the OSA-0.4-20% provides more aldehyde groups for cross-linking reaction. Figure 3e depicts the effect of the HACC/OSA comixing ratio on the duration of the HACC/OSA hydrogel

gelation when the HACC concentration and OSA-0.4 concentration are constant. When the blend ratio of HACC and OSA-0.4 was 2:1, the gelation time was 320 ± 43 s; as the mixing ratio increased to 5:1, the gelation time dropped to 194 ± 40 s. This result indicated that the increased content of HACC contributed to the rapid formation of the hydrogel. The other criteria specified above were maintained constant. It was discovered that altering the OSA-1 concentration significantly affects the gelation time (Figure 3f). When the concentration of OSA-1 was increased from 5 to 10 wt %, the gelation time of the hydrogel rapidly decreased from 687 ± 18 to 74 ± 9 s. As the concentration of OSA continues to increase, the gelation time was prolonged, and when it increased up to 20 wt %, the gelation time extended to 572 ± 28 s. This may be because when the oxidation degree of OSA-1 increased, more aldehyde groups were provided for the reaction with the amino groups of HACC to form a network structure, so the gelation time was shortened; however, when the concentration of OSA-1 exceeded 10 wt %, the aldehyde groups in the solution become saturated, resulting in prolonged gelation time, which is similar to the previous paper reported by Fan.[42] The shorter gelation time provides sufficient conditions for the application of hydrogels in the medical field.

3.4. Mechanical Testing Results. The stress−strain and compression modulus of hydrogels were evaluated to illustrate their mechanical characteristics (Figures 4 and 5). The concentration of HACC and the blending ratio of the two parts were fixed as 5 wt % and 5:1, respectively; then, the effect of the OD and concentration of OSA on the mechanical properties of hydrogel was analyzed scientifically. The
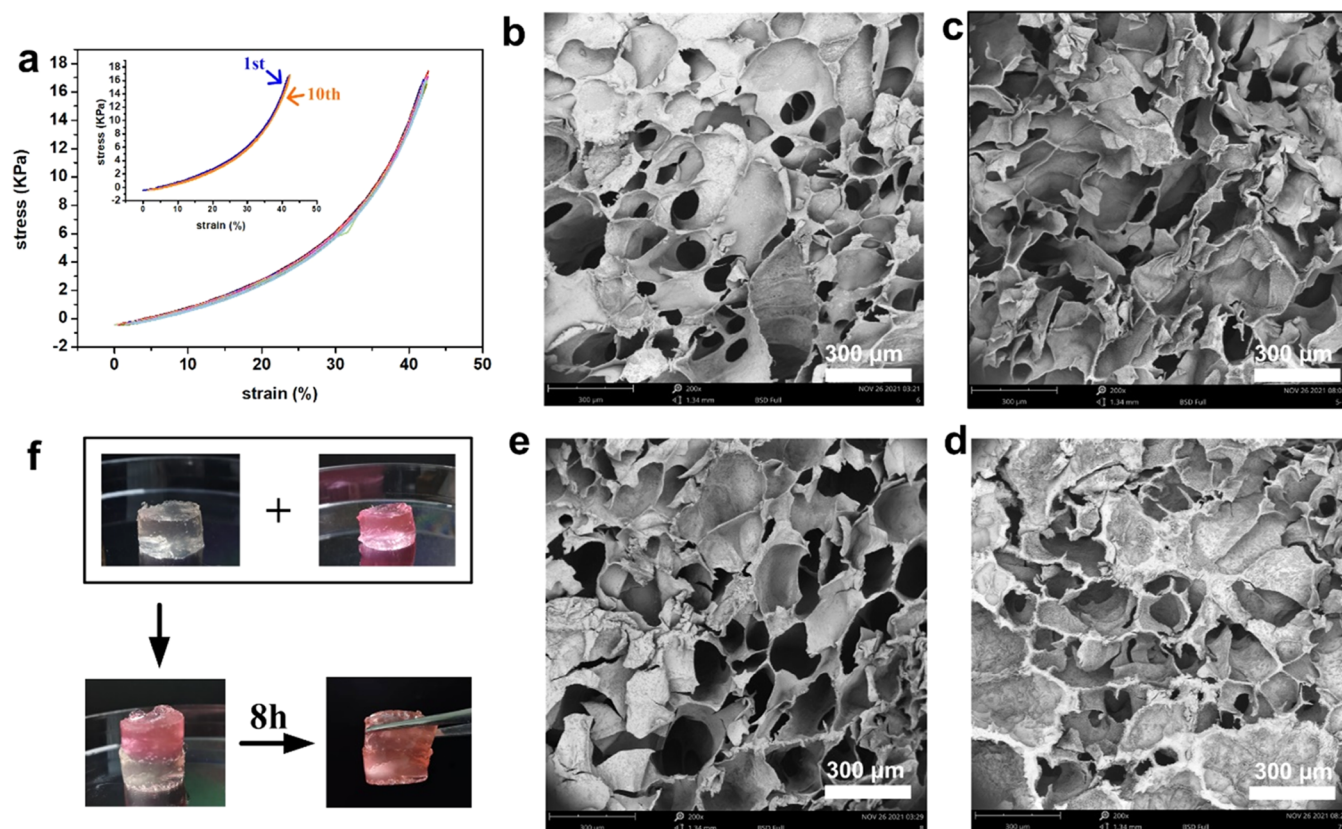
Figure 6. (a) Strain−strain curve of 10 successive loading−unloading cycles of HACC/OSA-1-10% hydrogels under 40%. SEM of the HACC/OSA hydrogels. (b) HACC/OSA-1-5%, (c) HACC/OSA-1-10%, (d) HACC/OSA-1-15%, (e) HACC/OSA-1-20%, and (f) photographs of the self-healing properties of the HACC/OSA-1-10% hydrogel.

compressive fracture stress and compressive modulus of hydrogel increased with the increase of the OSA-0.4 concentration, and the HACC/OSA-0.4-20% of the fracture stress could reach 224 kPa and the compressive modulus was 22.5 kPa, which was much greater than that of the other sample groups, and it had the highest stiffness among the samples (Figure 4). Compared with Geng's ionic cross-linked hydrogel with a compressive strength of about 27 kPa, our hydrogel is about 10 times higher and shows excellent mechanical properties.[21] And compared to the compression strength of the similar Schiff base cross-linked O-HACC/PVA/GO hydrogels (1.5 kPa), HACC/OSA-0.4-20% has a hundred times higher compressive strength.[43]

The change in the concentration of OSA-1 had few effects on the compressive fracture stress of the hydrogel, which was almost always maintained at about 110−155 kPa, while the compressive modulus of the HACC/OSA-1-20% hydrogel sample was 25.3 ± 2.4 kPa, which was significantly higher than that of the other sample groups. The mechanical results show that all samples show typical properties of elastic hydrogels, where low compressive stresses lead to high deformation, which we also found in the mechanical tests. Figures 4b and 5b show the rapid recovery of deformation of HACC/OSA-0.4-10% and HACC/OSA-1-10% hydrogels after compression with a finger, respectively. In summary, the OD of OSA has an effect on the compressive properties of the hydrogels, which may be due to the different densities and structural stabilities of the increased aldehyde groups contained in OSA cross-linked with the amino groups of the HACC. In conclusion, the

excellent mechanical properties of HACC/OSA hydrogels provide a good basis for the application of biomaterials.

A vertical compression release test was performed on a cylindrical sample of HACC/OSA-1-10% hydrogel in order to evaluate its shape recovery ability. As shown in Figure 6a, the representative stress−strain curves for 10 tests of cyclic compression release at a strain of 40%. The cyclic stress−strain curves exhibited hysteresis, indicating a phase angle between the strain change and the stress change in the hydrogel.[44,45] Comparing the previously reported hydrogels, the hysteresis lines of HACC/OSA-1-10% hydrogels compressed by multiple cycles were found to be almost identical, indicating that the hydrogels have excellent elasticity.

The above experimental results were combined, the HACC concentration was fixed at 5 wt %, the OD of OSA was fixed at 1, and the blending ratio was fixed at 5:1;, the HACC/OSA-1 with different concentrations of OSA-1 were chosen for the next experimental tests.[46]

3.5. Morphological Characterization and Self-Healing of Hydrogel. The morphology and microstructure of the hydrogels after lyophilization were analyzed through SEM images (Figure 6b−e). It can be clearly observed that the obtained hydrogel displays a continuous porous network structure, which is similar to other polymer hydrogel structures.[47] All four hydrogels have a highly porous structure with a continuous distribution of pore morphology (Figure 2). The pore size of the hydrogel is closely related to the amount of solids added.[48] Image J was used to perform the aperture calculation. The pore size of the hydrogel gradually decreased from 231 to 167 μm as the concentration of OSA-1 increased

Table 1. Pore Size of HACC/OSA Hydrogels

sample	HACC/OSA-1-5%	HACC/OSA-1-10%	HACC/OSA-1-15%	HACC/OSA-1-20%
pore size (μm)	231 ± 3	199 ± 7^a	176 ± 11^a	167 ± 6^a

[a]Different letters in the table indicate significant differences ($p < 0.05$, $n = 3$ per group).
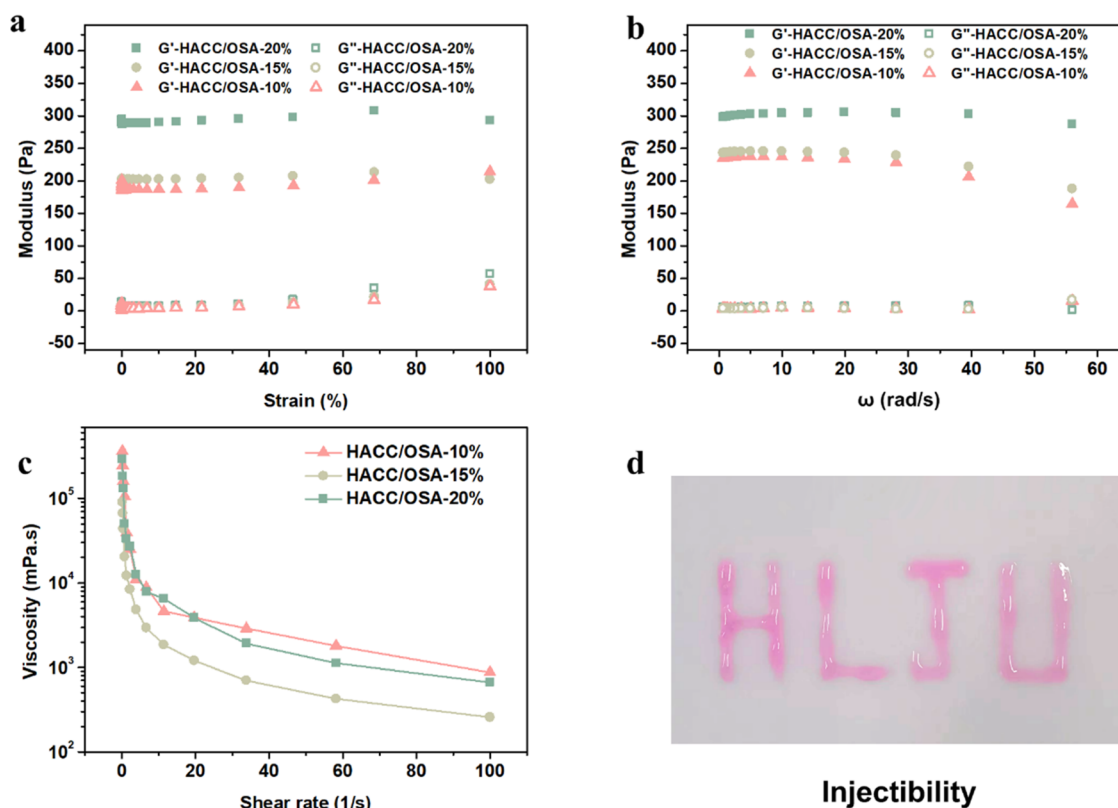

Figure 7. (a) Storage modulus and loss modulus were measured by the strain sweep test; (b) storage modulus and loss modulus were measured by the frequency sweep test. (c) Viscosity as a function of shear rate is demonstrated via a flow scan test. (d) Injection of a HACC/OSA-10% hydrogel.

(as shown in Table 1). It can be seen from the SEM images that the pore sizes of HACC/OSA-1-10%, HACC/OSA-1-15%, and HACC/OSA-1-20% are significantly smaller than that of HACC/OSA-1-5%, indicating that their concentration of solids is higher. In addition, the porous structure is beneficial to the exchange of nutrients, air, and water, as well as the excretion of metabolic waste.

The self-healing behavior of hydrogels was tested using direct visual inspection. As shown in Figure 6f, cylindrical hydrogels containing RB and those without RB were prepared separately, and these two hydrogels were stacked together at room temperature. After 3 h, the boundary between these two pieces of hydrogel turned to be blurred and obscure. Moreover, after 8 h, half of the hydrogel stained with RB completely fused to the other half transparent hydrogel, and these two hydrogel sheets merged together. The final self-healing disc was strong enough to maintain the overlapping weight when picked up with tweezers, which may be due to the formation of reversible imine bonds after the action of Schiff bases between the two hydrogels, leading to the self-healing phenomenon that occurred. The self-healing properties of the hydrogel are beneficial to completely cover the irregular tissue defect sites, avoiding cracks and gaps during the process of tissue recovery.

3.6. Rheological Characterization. The rheological behavior of HACC/OSA hydrogels is shown in Figure 7, where different concentrations of hydrogels show different rheological properties. The strain scan acquired during in situ gelation is shown in Figure 7a; the G'-HACC/OSA-1-20% hydrogel was slightly higher than the other two groups, indicating that the stiffness of the hydrogel increases with increasing OSA concentration. And it can be observed that the hydrogel is viscoelastic even when subjected to 100% strain since the hydrogel's G' is much bigger than its G'' value. Monitoring the storage modulus (G') and loss modulus (G'') at angular frequencies at 25 °C allowed researchers to determine the hydrogel's rheological characteristics (Figure 7b). Each hydrogel group exhibited a stable elastic modulus, and the increase in modulus was directly related to the OSA content in the compositions, and the hydrogels would be stronger when the OSA content increased.

In general, the hydrogel's fluctuation in G' with frequency is almost constant and significantly greater than the equivalent G''. This rheological behavior of the hydrogel predicts the formation of a material ideal for wound healing with good elastic and solid characteristics since the hydrogel's dominant tendency is elastic. The shear thinning properties of the hydrogel were studied using a shear rate of $0.15-100$ s^{-1} at a constant strain (Figure 7c). The excellent shear thinning ability
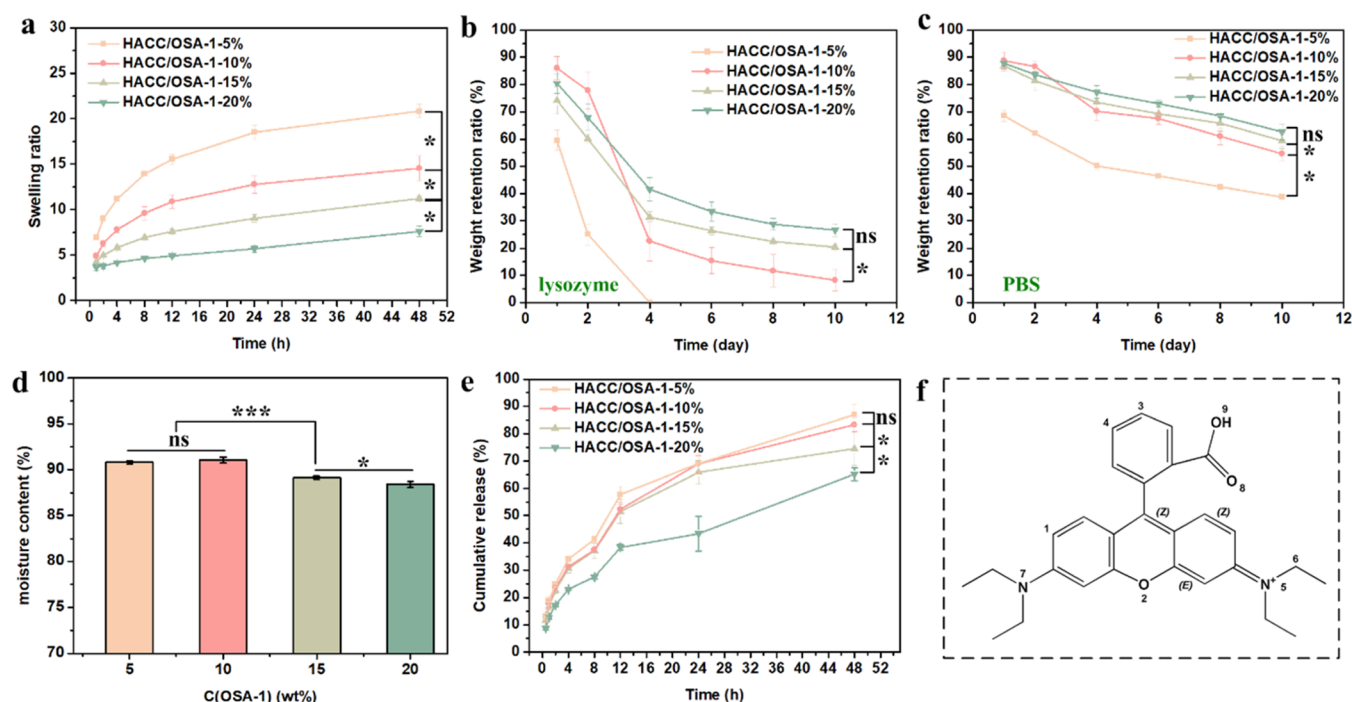
Figure 8. (a) Swelling rate versus time in hydrogels containing different concentrations of OSA. (b) and (c) The degradation weight retention rate of hydrogels containing different concentrations of OSA varied with time in lysozyme and PBS. (d) Moisture content test of hydrogels with different concentrations of OSA-1. (e) The release profiles of rhodamine B from hydrogel in PBS. (f) Structural formula of rhodamine B. Data are expressed as mean $\pm$ SD (n = 3; ns = no significance, *p < 0.05,***p < 0.001).

of these hydrogels is demonstrated, which is required for the injectability of the hydrogels, as evidenced by the observation that the viscosity of the hydrogels reduced with increasing shear rate.[25,30] With the increase of shear rate, the viscosity of HACC/OSA-1-10% hydrogel was slightly higher than the other two groups, which may be the result of the rapid cross-linking reaction of HACC/OSA-1-10% hydrogel and the increase of viscosity after forming hydrogel was less affected by shear damage. The macroscopic injectability of the HACC/OSA-10% hydrogel is further confirmed by Figure 7d. More specifically, the HACC/OSA-1-10% system can be continuously injected on the PP plastic plate with a 1 mL syringe and the formed "HLJU" font can be maintained in the hydrogel state.[30]

3.7. Swelling, Degradation, and Moisture Content of Hydrogel. Figure 8a shows the swelling kinetics of HACC/OSA-1 hydrogels with different concentrations of OSA-1. The swelling rate of all samples increased with the time of incubation. The results showed that the swelling ratio of the HACC/OSA-1-5% hydrogel was significantly higher than that of the other groups, and the swelling ratio reached 20.82 after 48 h. The results may be attributed to the fact that both HACC and OSA have favorable water absorption properties; when the concentration of OSA is 5 wt %, the two components have fewer cross-linked sites and occupy less space in the hydrogel system after forming the hydrogel. The HACC has good water absorption ability, which will increase the water absorption in the highly absorbent hydrogel network, resulting in a good swelling performance of the hydrogel.[49]

The degradation ability of hydrogels is an essential feature for biomedical applications; therefore, the degradation behavior of hydrogels was evaluated. The weight retention of several hydrogels throughout a 10 day degrading period is depicted in Figure 8b. During the first 4 days of degradation,

all hydrogels showed a rapid degradation trend, in which the HACC/OSA-1-5% hydrogel was completely degraded and it could be observed that the hydrogel had completely fused with the solution; HACC/OSA-1-10% hydrogels showed high weight retention during the first 2 days of degradation, which may be due to the high cross-link density protecting them from the degradation by lysozyme less, but on day 4, it showed a significant and rapid mass reduction of 22.46%, and all three hydrogel groups showed intact morphology and reduced volume. Next, the rest of the three groups demonstrated consistent mass reduction and fragmentation of the samples over the course of the process from 4 to 10 days. The mass retention rate of the HACC/OSA-1-10% hydrogel after 10 days was only 8.16%, which was significantly lower than the rates of the other two groups of hydrogels. Figure 8c shows the degradation weight retention of hydrogels in PBS (pH = 7.4); as a control, it can be seen that the degradation rate of all hydrogel groups was slowed down under the same degradation condition without lysozyme. The results show that the degradation rate decreases with increasing cross-linking of the hydrogel under the effect of lysozyme on HACC, so the smaller the concentration of OSA, the easier the hydrogel is to degrade, which is desirable for materials with biomedical applications.

Figure 8c shows the moisture content of the hydrogels synthesized with different OSA contents, and it can be seen that the moisture content of the HACC/OSA hydrogels was always maintained at about 91% when the OSA content was increased from 5 to 10 wt %, while the OSA content was 20 wt %, the moisture content of the HACC/OSA hydrogel was 88.42%, significantly lower than other hydrogel samples. This could be a result of the hydrogel's low cross-link density and high capacity for storing water in its network structure. It is shown that the HACC/OSA hydrogel can store a large amount
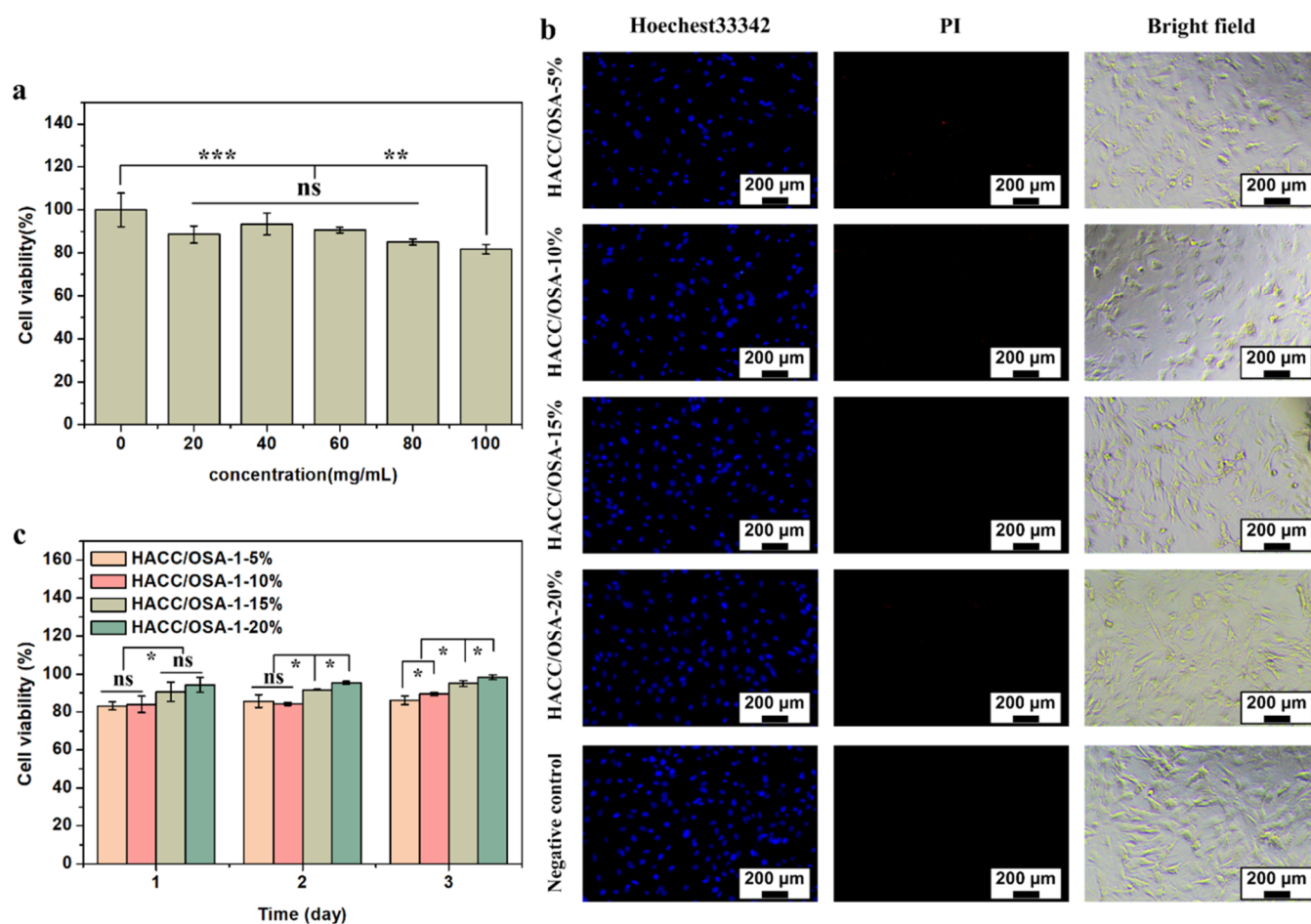
Figure 9. (a) Cell viability after culturing cells with different concentrations of HACC/OSA-1-15% hydrogel extract solution for 24 h. (b) The Hoechest33342/PI staining of BMSC cells after treatment with different sample extracts. (c) Cell viability of different hydrogel extract solutions (n = 3; ns = not significant, *p < 0.05).

of water, has excellent water storage performance, can effectively maintain the moist healing environment of wound tissue and other parts, and promote the exchange of body fluids, which can lay a good foundation for the application of biomaterials for wound repair.

3.8. Drug Release. The drug release ability of the hydrogels was investigated using RB as a model drug. Figure 8e shows the cumulative release rate of RB from different HACC/OSA hydrogels during 48 h. The release rate of RB decreased with an increase of concentration of OSA, where the cumulative release rate of RB from HACC/OSA-1-5% hydrogels at 48 h was 87%, which was significantly higher than that of HACC/OSA-1-20% hydrogels with a 65% release rate. The result may be attributed to the fact that the hydrogels have different structures, swelling ratios, and degradation behaviors. Larger apertures are more conducive to drug diffusion, and the higher swelling ratio and the faster degradation rate make it easier for the embedded drug to escape from the hydrogel.[50] In addition, because the RB is a cationic dye (Figure 8f),[51] when the concentration of the negatively charged OSA increases, it could bind more RB and thus reduce the release of RB. In conclusion, the HACC/OSA hydrogel proved to have some potential ability for drug delivery applications.

3.9. Cytotoxicity of HACC/OSA Hydrogels. In this study, hydrogel extraction was applied to examine hydrogel

cytotoxicity, and BMSC cell viability was assessed using the CCK-8 test as well as Hoechst 33342 and PI staining. First, through evaluating the above experimental results to select HACC/OSA-1-15% hydrogel samples for cell viability tests with different concentrations of hydrogel extract solution in culture, we discovered that the cell proliferation rates were above 80% (Figure 9a). The following sample extract concentration of 60 mg/mL was chosen for cytotoxicity testing since it was thought that a concentration of hydrogel extract that was too low would provide incorrect test findings. Figure 9b depicts Hoechest33342 and PI fluorescence pictures of cells cultivated in hydrogel extract solution on the third day. To examine cell growth, normal cells are dyed low blue and dead cells are labeled red. In all sample groups, the extract solution had no significant effect on the morphology of BMSCs, while the number of cells in the HACC/OSA-1-5% hydrogel samples was slightly lower than in the other sample groups. Figure 9c shows the viability of BMSC cells at different time points after being cultured in different hydrogel extraction solutions. On the first day of culture, the cell survival rates of HACC/OSA-1-15% and HACC/OSA-1-20% hydrogel groups were significantly higher than the other two, about 90 and 94%, respectively. On the second day, cell viability increased significantly in the former two groups of hydrogel extract cultures, 85 and 84%, and was significantly higher in the HACC/OSA-1-20% hydrogel group than in the other groups,
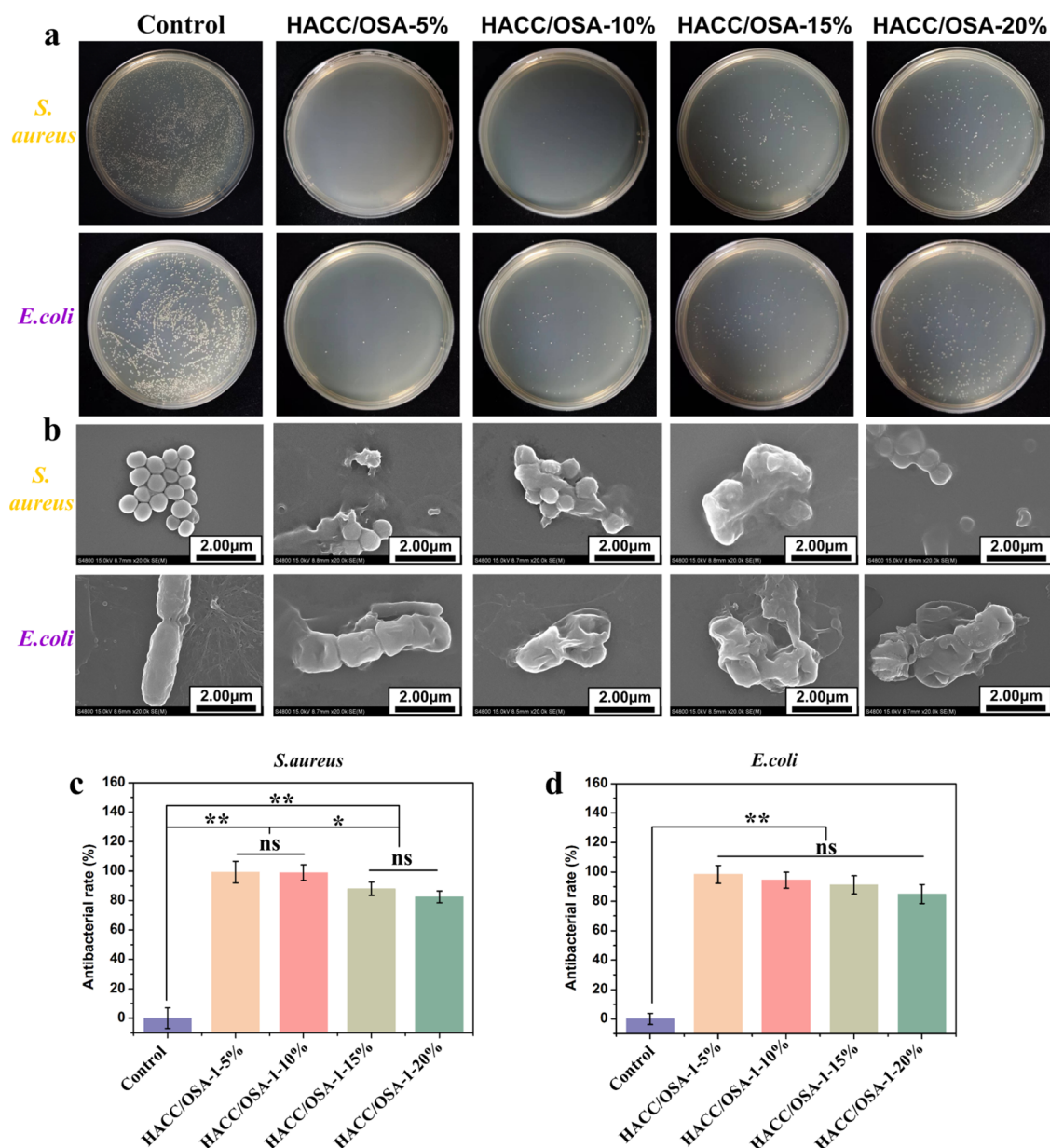
Figure 10. (a) Colony growth of bacterial suspensions after 18 h of incubation on agar plates; (b) SEM images of bacterial morphology on plates; and (c) and (d) corresponding antibacterial rates against *E. coli* and *S. aureus* ($n = 3$; ns = not significant, $*p < 0.05$, $**p < 0.01$).

at 95%. On the third day, significant variation in cell viability among groups was seen, in which the cell viability of the HACC/OSA-1-20% hydrogel group was still over 95%, while the cell survival rate of the HACC/OSA-1-5% hydrogel group was lower than the other three groups, but in Figure 9b PI staining, there were not a large number of dead cells, indicating that the hydrogel was not potentially cytotoxic. The lower cell activity in the ACC/OSA-1-5% hydrogel group may be due to the fact that the BMSC cells themselves are more sensitive and the solid extract of the hydrogel has some negative effects on the cells. These results indicate that these self-cross-linked hydrogels have good biocompatibility.[30]

3.10. Antibacterial Ability of the HACC/OSA Hydrogels. As biomaterials used in the body, the antibacterial ability is very important; it helps in reducing the number of pathogens, as well as decreasing the inflammatory response and exudate formation at the injury site. *E. coli* and *S. aureus*

are common pathogenic microorganisms in injury sites and are thus used in antibacterial tests. As shown in Figure 10a, both HACC/OSA hydrogels showed excellent inhibition of *S. aureus* and *E. coli*, with almost no colonies formed on HACC/OSA-1-5% and HACC/OSA-1-10% hydrogel plates, and their antibacterial rates were up to ~98% for both bacteria (Figure 10c,d), while HACC/OSA-1-10% hydrogels showed slightly lower antibacterial rate against *E. coli* at 94%. As the concentration of OSA increased, the colonies on the agar plates increased, and the antibacterial rate decreased to about 82% against *S. aureus* and 85% against *E. coli*, indicating that the inhibition of both bacteria is weakened as the amount of HACC is relatively reduced. Overall, HACC/OSA hydrogel has excellent antibacterial ability while showing a weaker antibacterial effect on Gram-negative bacteria. These findings are consistent with previous literatures reporting that HACC has a stronger antibacterial effect on Gram-positive bacteria.[52]

Furthermore, the morphology of bacteria treated with different hydrogels was observed by SEM. The control group showed a normal appearance with viable bacteria (Figure 10b). The remaining four groups pose a wrinkle and collapsed morphology and lost their physiological structure, which could induce bacterial cell membrane damage and content outflow and ultimately lead to bacterial death. The inhibitory activity of HACC/OSA hydrogels against both bacteria was mainly dependent on the interaction of polycationic HACC with bacterial cell membranes, which resulted in the disruption of bacterial cell membranes.[29] The results revealed that the HACC/OSA hydrogels have great antibacterial properties, which could be conducive for potential application in the field of biomedical carriers and wound dressing.

4. CONCLUSIONS

In summary, a novel polysaccharide hydrogel (HACC/OSA hydrogel) was successfully prepared by Schiff base self-cross-linking. First, the flocculation of hydrogel precursor was solved by adding counterions. By changing the OD of OSA, concentrations of the HACC and OSA, and blend ratio of the HACC/OSA, the hydrogel exhibited different gel formation kinetics, and the HACC/OSA can be formed ranging from 74 to 572 s, The formed hydrogel had an interconnected porous structure and showed improved mechanical property and elasticity. What's more, the hydrogel possessed self-healing ability, excellent swelling ability, degradability, cytocompatibility, and antibacterial ability. It also has a good sustained release effect on RB. These parameters can be modulated to accommodate various biological requirements. The HACC/OSA hydrogels prepared in this work have the potential capacity for biomedical carriers or antibacterial wound dressing applications.

■ ASSOCIATED CONTENT

Ⓢ Supporting Information

The Supporting Information is available free of charge at https://pubs.acs.org/doi/10.1021/acsomega.3c01401.

> Experimental section; degree of substitution (DS) of HACC; determination of the oxidation degree; and the flocculation disappears after adding positive counterions from NaCl to the hydrogel (PDF)

■ AUTHOR INFORMATION

Corresponding Authors

Zheng Jin − College of Chemistry and Material Sciences & School of Life Sciences, Heilongjiang University, Harbin, Heilongjiang 150080, China; Zhejiang Provincial Key Laboratory of Plant Evolutionary Ecology and Conservation, School of Life Sciences, Taizhou University, Taizhou, Zhejiang 318000, China; ⓞ orcid.org/0000-0003-2537-6664; Email: jinzhengdvd@163.com

Yiyu Wang − Zhejiang Provincial Key Laboratory of Plant Evolutionary Ecology and Conservation, School of Life Sciences, Taizhou University, Taizhou, Zhejiang 318000, China; ⓞ orcid.org/0000-0001-6640-2107; Email: yiyiyuyu.7@163.com

Kai Zhao − College of Chemistry and Material Sciences & School of Life Sciences, Heilongjiang University, Harbin, Heilongjiang 150080, China; Zhejiang Provincial Key Laboratory of Plant Evolutionary Ecology and Conservation, School of Life Sciences, Taizhou University, Taizhou, Zhejiang 318000, China; ⓞ orcid.org/0000-0001-6139-1912; Email: zybin395@126.com

Authors

Guiting Yu − College of Chemistry and Material Sciences & School of Life Sciences, Heilongjiang University, Harbin, Heilongjiang 150080, China

Chunqing Niu − Department of Mechanical Engineering and Robotics, Faculty of Textile Science and Technology, Shinshu University, Ueda, Nagano 386-8567, Japan

Jiali Liu − College of Chemistry and Material Sciences & School of Life Sciences, Heilongjiang University, Harbin, Heilongjiang 150080, China

Jue Wu − College of Chemistry and Material Sciences & School of Life Sciences, Heilongjiang University, Harbin, Heilongjiang 150080, China; Zhejiang Provincial Key Laboratory of Plant Evolutionary Ecology and Conservation, School of Life Sciences, Taizhou University, Taizhou, Zhejiang 318000, China

Complete contact information is available at:
https://pubs.acs.org/10.1021/acsomega.3c01401

Notes

The authors declare no competing financial interest.

■ ACKNOWLEDGMENTS

■ REFERENCES

(1) Chen, F. M.; Liu, X. H. Advancing biomaterials of human origin for tissue engineering. *Prog. Polym. Sci.* **2016**, *53*, 86−168.

(2) Zhao, X. H.; Chen, X. Y.; Yuk, H.; Lin, S. T.; Liu, X. Y.; Parada, G. Soft Materials by Design: Unconventional Polymer Networks Give Extreme Properties. *Chem. Rev.* **2021**, *121*, 4309−4372.

(3) Naghizadeh, Z.; Karkhaneh, A.; Khojasteh, A. Self-crosslinking effect of chitosan and gelatin on alginate based hydrogels: Injectable in situ forming scaffolds. *Mater. Sci. Eng., C* **2018**, *89*, 256−264.

(4) Gan, S. C.; Xu, B.; Zhang, X.; Zhao, J. H.; Rong, J. H. Chitosan derivative-based double network hydrogels with high strength, high fracture toughness and tunable mechanics. *Int. J. Biol. Macromol.* **2019**, *137*, 495−503.

(5) Park, S. H.; Ju, H. J.; Ji, Y. B.; Shah, M.; Min, B. H.; Choi, H. S.; Choi, S.; Kim, M. S. Endogenous Stem Cell-Based In Situ Tissue Regeneration Using Electrostatically Interactive Hydrogel with a Newly Discovered Substance P Analog and VEGF-Mimicking Peptide. *Small* **2021**, *17*, No. 2103244.

(6) Xu, J. Y.; Liu, X.; Ren, X. Y.; Gao, G. H. The role of chemical and physical crosslinking in different deformation stages of hybrid hydrogels. *Eur. Polym. J.* **2018**, *100*, 86−95.

(7) Zerbinati, N.; Esposito, C.; Cipolla, G.; Calligaro, A.; Monticelli, D.; Martina, V.; Golubovic, M.; Binic, I.; Sigova, J.; Gallo, A. L.; et al. Chemical and mechanical characterization of hyaluronic acid hydrogel cross-linked with poly(ethylene glycol) and its use in dermatology. *Dermatol. Ther.* **2020**, *33*, No. e13747.

(8) Kim, S.; Jeong, D.; Lee, H.; Kim, D.; Jung, S. Succinoglycan dialdehyde-reinforced gelatin hydrogels with toughness and thermal stability. *Int. J. Biol. Macromol.* **2020**, *149*, 281−289.

(9) Hoang, H. T.; Vu, T. T.; Karthika, V.; Jo, S.-H.; Jo, Y.-J.; Seo, J.-W.; Oh, C.-W.; Park, S.-H.; Lim, K. T. Dual cross-linked chitosan/

alginate hydrogels prepared by Nb-Tz 'click' reaction for pH responsive drug delivery. *Carbohydr. Polym.* **2022**, *288*, No. 119389.

(10) Xue, X.; Hu, Y.; Wang, S. C.; Chen, X.; Jiang, Y. Y.; Su, J. C. Fabrication of physical and chemical crosslinked hydrogels for bone tissue engineering. *Bioact. Mater.* **2022**, *12*, 327−339.

(11) Yao, Y.; Wang, P. L.; Li, X.; Xu, Y.; Lu, G. G.; Jiang, Q.; Sun, Y.; Fan, Y. J.; Zhang, X. D. A di-self-crosslinking hyaluronan-based hydrogel combined with type I collagen to construct a biomimetic injectable cartilage-filling scaffold. *Acta Biomater.* **2020**, *111*, 197−207.

(12) Yang, Y.; Liang, Y.; Chen, J.; Duan, X.; Guo, B. Mussel-inspired adhesive antioxidant antibacterial hemostatic composite hydrogel wound dressing via photo-polymerization for infected skin wound healing. *Bioact. Mater.* **2022**, *8*, 341−354.

(13) Kim, Y. M.; Potta, T.; Park, K. H.; Song, S. C. Temperature responsive chemical crosslinkable UV pretreated hydrogel for application to injectable tissue regeneration system via differentiations of encapsulated hMSCs. *Biomaterials* **2017**, *112*, 248−256.

(14) Chen, H. N.; Xing, X. D.; Tan, H. P.; Jia, Y.; Zhou, T. L.; Chen, Y.; Ling, Z. H.; Hu, X. H. Covalently antibacterial alginate-chitosan hydrogel dressing integrated gelatin microspheres containing tetracycline hydrochloride for wound healing. *Mater. Sci. Eng., C* **2017**, *70*, 287−295.

(15) Wang, H. C.; Chen, X. Q.; Wen, Y. S.; Li, D. Z.; Sun, X. Y.; Liu, Z. W.; Yan, H. Q.; Lin, Q. A Study on the Correlation between the Oxidation Degree of Oxidized Sodium Alginate on Its Degradability and Gelation. *Polymers* **2022**, *14*, 1679.

(16) Wang, L.; Zhou, W. F.; Wang, Q. G.; Xu, C.; Tang, Q.; Yang, H. An Injectable, Dual Responsive, and Self-Healing Hydrogel Based on Oxidized Sodium Alginate and Hydrazide-Modified Poly-(ethyleneglycol). *Molecules* **2018**, *23*, 546.

(17) Feng, X. L.; Zhang, X. F.; Li, S. Q.; Zheng, Y. Q.; Shi, X. N.; Li, F.; Guo, S. B.; Yang, J. M. Preparation of aminated fish scale collagen and oxidized sodium alginate hybrid hydrogel for enhanced full-thickness wound healing. *Int. J. Biol. Macromol.* **2020**, *164*, 626−637.

(18) Yao, Q. Q.; Liu, Y.; Pan, Y. N.; Li, Y. J.; Xu, L. M.; Zhong, Y. M.; Wang, W.; Zuo, J. Y.; Yu, H.; Lv, Z. R.; et al. Long-term induction of endogenous BMPs growth factor from antibacterial dual network hydrogels for fast large bone defect repair. *J. Colloid Interface Sci.* **2022**, *607*, 1500−1515.

(19) Liang, L. M.; Hou, T. T.; Ouyang, Q. Q.; Xie, L.; Zhong, S. Y.; Li, P. W.; Li, S. D.; Li, C. P. Antimicrobial sodium alginate dressing immobilized with polydopamine-silver composite nanospheres. *Composites, Part B* **2020**, *188*, No. 107877.

(20) Pasaribu, S. P.; Kaban, J.; Ginting, M.; Silalahi, J. Preparation of In Situ Cross-Linked N-Maleoyl Chitosan-Oxidized Sodium Alginate Hydrogels for Drug Delivery Applications. *Open Access Maced. J. Med. Sci.* **2019**, *7*, 3546−3553.

(21) Geng, Z. J.; Ji, Y. X.; Yu, S.; Liu, Q. F.; Zhou, Z. B.; Guo, C. P.; Lu, D. H.; Pei, D. T. Preparation and characterization of a dual cross-linking injectable hydrogel based on sodium alginate and chitosan quaternary ammonium salt. *Carbohydr. Res.* **2021**, *507*, No. 108389.

(22) Pita-López, M. L.; Fletes-Vargas, G.; Espinosa-Andrews, H.; Rodríguez-Rodríguez, R. Physically cross-linked chitosan-based hydrogels for tissue engineering applications: A state-of-the-art review. *Eur. Polym. J.* **2021**, *145*, No. 110176.

(23) Zhou, L.; Dai, C.; Fan, L.; Jiang, Y. H.; Liu, C.; Zhou, Z. N.; Guan, P. F.; Tian, Y.; Xing, J.; Li, X. J.; et al. Injectable Self-Healing Natural Biopolymer-Based Hydrogel Adhesive with Thermorespon-sive Reversible Adhesion for Minimally Invasive Surgery. *Adv. Funct. Mater.* **2021**, *31*, No. 2007457.

(24) Pandit, A. H.; Nisar, S.; Imtiyaz, K.; Nadeem, M.; Mazumdar, N.; Rizvi, M. M. A.; Ahmad, S. Injectable, Self-Healing, and Biocompatible N,O-Carboxymethyl Chitosan/Multialdehyde Guar Gum Hydrogels for Sustained Anticancer Drug Delivery. *Biomacro-molecules* **2021**, *22*, 3731−3745.

(25) Yuan, N. X.; Xu, L.; Xu, B.; Zhao, J. H.; Rong, J. H. Chitosan derivative-based self-healable hydrogels with enhanced mechanical

properties by high-density dynamic ionic interactions. *Carbohydr. Polym.* **2018**, *193*, 259−267.

(26) Qi, X. L.; Xiang, Y. J.; Cai, E.; You, S. Y.; Gao, T.; Lan, Y. L.; Deng, H.; Li, Z. P.; Hu, R. D.; Shen, J. L. All-in-one: Harnessing multifunctional injectable natural hydrogels for ordered therapy of bacteria-infected diabetic wounds. *Chem. Eng. J.* **2022**, *439*, No. 135691.

(27) Wang, W. Q.; Meng, Q. Y.; Li, Q.; Liu, J. B.; Zhou, M.; Jin, Z.; Zhao, K. Chitosan Derivatives and Their Application in Biomedicine. *Int. J. Biol. Macromol.* **2020**, *21*, 487.

(28) Hoque, J.; Prakash, R. G.; Paramanandham, K.; Shome, B. R.; Haldar, J. Biocompatible Injectable Hydrogel with Potent Wound Healing and Antibacterial Properties. *Mol. Pharmaceutics* **2017**, *14*, 1218−1230.

(29) Liang, Y. Q.; Li, Z. L.; Huang, Y.; Yu, R.; Guo, B. L. Dual-Dynamic-Bond Cross-Linked Antibacterial Adhesive Hydrogel Sealants with On-Demand Removability for Post-Wound-Closure and Infected Wound Healing. *ACS Nano* **2021**, *15*, 7078−7093.

(30) Wang, Y. Y.; Niu, C. Q.; Shi, J.; Yu, W. L.; Zhu, C. H.; Zhang, Q.; Mizuno, M. A Carbodiimide Cross-Linked Silk Fibroin/Sodium Alginate Composite Hydrogel with Tunable Properties for Sustained Drug Delivery. *Macromol. Mater. Eng.* **2021**, *306*, No. 2100470.

(31) Niu, C.; Liu, X.; Wang, Y.; Li, X.; Shi, J. Photothermal-modulated drug release from a composite hydrogel based on silk fibroin and sodium alginate. *Eur. Polym. J.* **2021**, *146*, No. 110267.

(32) Xu, C.; Wang, S.; Liu, L. L.; Yu, S. C.; Wu, X. P.; Dai, H. L. Manipulating Mesenchymal Stem Cells Differentiation Under Sinus-oidal Electromagnetic Fields Using Intracellular Superparamagnetic Nanoparticles. *J. Biomed. Nanotechnol.* **2019**, *15*, 301−310.

(33) Xu, C.; Xu, Y.; Yang, M.; Chang, Y.; Nie, A.; Liu, Z.; Wang, J.; Luo, Z. Black-Phosphorus-Incorporated Hydrogel as a Conductive and Biodegradable Platform for Enhancement of the Neural Differentiation of Mesenchymal Stem Cells. *Adv. Funct. Mater.* **2020**, *30*, No. 2000177.

(34) Zhou, L.; Pi, W.; Cheng, S. Y.; Gu, Z.; Zhang, K. X.; Min, T. T.; Zhang, W. M.; Du, H. W.; Zhang, P. X.; Wen, Y. Q. Multifunctional DNA hydrogels with hydrocolloid-cotton structure for regeneration of diabetic infectious wounds. *Adv. Funct. Mater.* **2021**, *31*, No. 2106167.

(35) Jin, Z.; Li, W.; Cao, H. W.; Zhang, X.; Chen, G.; Wu, H.; Guo, C.; Zhang, H. K.; Kang, H.; Wang, Y. F.; Wang, Y.; Zhao, K. Antimicrobial activity and cytotoxicity of N-2-HACC and character-ization of nanoparticles with N-2-HACC and CMC as a vaccine carrier. *Chem. Eng. J.* **2013**, *221*, 331−341.

(36) Fu, C. M.; Jin, Z.; Zhao, K. Protective Effect of Composite Hydrogel Based on Hydroxypropyl Trimethylammonium Chloride Chitosan on Skin Photodamage. *ACS Appl. Polym. Mater.* **2022**, *4*, 7587−7598.

(37) Zhang, Z. X.; Liow, S. S.; Xue, K.; Zhang, C. K.; Li, Z. B.; Loh, X. J. Autonomous chitosan-based self-healing hydrogel formed through noncovalent interactions. *ACS Appl. Polym. Mater.* **2019**, *1*, 1769−1777.

(38) Yin, X.; Xie, H. G.; Li, R. X.; Yan, S. G.; Yin, H. Regulating association strength between quaternary ammonium chitosan and sodium alginate via hydration. *Carbohydr. Polym.* **2021**, *255*, No. 117390.

(39) Rabelo, R. S.; Tavares, G. M.; Prata, A. S.; Hubinger, M. D. Complexation of chitosan with gum Arabic, sodium alginate and *κ*-carrageenan: Effects of pH, polymer ratio and salt concentration. *Carbohydr. Polym.* **2019**, *223*, No. 115120.

(40) Li, S. Z.; Pei, M. J.; Wan, T. T.; Yang, H. J.; Gu, S. J.; Tao, Y. Z.; Liu, X.; Zhou, Y. S.; Xu, W. L.; Xiao, P. Self-healing hyaluronic acid hydrogels based on dynamic Schiff base linkages as biomaterials. *Carbohydr. Polym.* **2020**, *250*, No. 116922.

(41) Lü, S.; Gao, C.; Xu, X.; Bai, X.; Duan, H. G.; Gao, N. N.; Feng, C.; Xiong, Y.; Liu, M. Z. Injectable and self-healing carbohydrate-based hydrogel for cell encapsulation. *ACS Appl. Mater. Interfaces* **2015**, *7*, 13029−13037.

(42) Fan, L. H.; Tan, C.; Wang, L. B.; Pan, X. R.; Cao, M.; Wen, F.; Xie, W. G.; Nie, M. Preparation, characterization and the effect of

carboxymethylated chitosan-cellulose derivatives hydrogels on wound healing. *J. Appl. Polym. Sci.* **2013**, *128*, 2789−2796.

(43) Cao, J. L.; He, G. H.; Ning, X. Q.; Chen, X. H.; Fan, L. H.; Yang, M.; Yin, Y. H.; Cai, W. Q. Preparation and properties of O-chitosan quaternary ammonium salt/polyvinyl alcohol/graphene oxide dual self-healing hydrogel. *Carbohydr. Polym.* **2022**, *287*, No. 119318.

(44) Dong, X. Y.; Guo, X.; Liu, Q. Y.; Zhao, Y. J.; Qi, H. B.; Zhai, W. Strong and Tough Conductive Organo-Hydrogels via Freeze-Casting Assisted Solution Substitution. *Adv. Funct. Mater.* **2022**, *32*, No. 2203610.

(45) Su, D. H.; Yao, M.; Liu, J.; Zhong, Y. M.; Chen, X.; Shao, Z. Z. Enhancing Mechanical Properties of Silk Fibroin Hydrogel through Restricting the Growth of beta-Sheet Domains. *ACS Appl. Mater. Interfaces* **2017**, *9*, 17490−17499.

(46) You, Y.; Xie, Y.; Jiang, Z. Injectable and biocompatible chitosan-alginic acid hydrogels. *Biomed. Mater.* **2019**, *14*, No. 025010.

(47) Xing, L.; Sun, J. C.; Tan, H. P.; Yuan, G. L.; Li, J. L.; Jia, Y.; Xiong, D. S.; Chen, G.; Lai, J. Z.; Ling, Z. H.; et al. Covalently polysaccharide-based alginate/chitosan hydrogel embedded alginate microspheres for BSA encapsulation and soft tissue engineering. *Int. J. Biol. Macromol.* **2019**, *127*, 340−348.

(48) Liu, X.; Peng, W. Z.; Wang, Y. Y.; Zhu, M. H.; Sun, T.; Peng, Q.; Zeng, Y.; Feng, B.; Lu, X.; Weng, J.; Wang, J. Synthesis of an RGD-grafted oxidized sodium alginate-N-succinyl chitosan hydrogel and an in vitro study of endothelial and osteogenic differentiation. *J. Mater. Chem. B* **2013**, *1*, 4484−4492.

(49) Xiong, Y.; Chen, L.; Liu, P.; Yu, T.; Lin, C.; Yan, C.; Hu, Y.; Zhou, W.; Sun, Y.; Panayi, A. C.; et al. All-in-One: Multifunctional Hydrogel Accelerates Oxidative Diabetic Wound Healing through Timed-Release of Exosome and Fibroblast Growth Factor. *Small* **2022**, *18*, No. 2104229.

(50) Liu, Y. Y.; Fan, Q.; Huo, Y.; Liu, C.; Li, B.; Li, Y. M. Construction of a mesoporous polydopamine@ GO/cellulose nano-fibril composite hydrogel with an encapsulation structure for controllable drug release and toxicity shielding. *ACS Appl. Mater. Interfaces* **2020**, *12*, 57410−57420.

(51) Kumar, V.; Singh, M.; Behera, K.; Pandey, S. Ionic liquid induced removal of Rhodamine B from water. *J. Mol. Liq.* **2020**, *319*, No. 114195.

(52) Xue, H.; Hu, L. C.; Xiong, Y.; Zhu, X. W.; Wei, C. Y.; Cao, F. Q.; Zhou, W.; Sun, Y.; Endo, Y.; Liu, M. F.; Liu, Y.; Liu, J.; Abududilibaier, A.; Chen, L.; Yan, C. C.; Mi, B. B.; Liu, G. H. Quaternized chitosan-Matrigel-polyacrylamide hydrogels as wound dressing for wound repair and regeneration. *Carbohydr. Polym.* **2019**, *226*, No. 115302.